

Headline Articles

Electric Field Effects on Electron Transfer between H^+ and Carbon-Based Electrode Surfaces: A DFT and Anderson–Newns Hamiltonian Analysis Study

Tsukuru Ohwaki, Takahiko Murai, and Koichi Yamashita*

Department of Chemical System Engineering, The University of Tokyo, 7-3-1 Hongo, Bunkyo-ku, Tokyo 113-8656

(Received June 6, 2001)

To investigate the nature of the characteristic properties (especially the wide potential window and the low background current) of boron-doped diamond electrodes, we discuss electric field effects on the electron transfer process between the diamond surface and a proton based on density functional theory (DFT) and Anderson–Newns Hamiltonian analysis. All of the necessary data for this analysis were obtained by a "finite-field DFT method" at the level of B3LYP/6-31G and natural bond orbital analysis (NBO). The diamond and graphite electrode surfaces were modeled by corresponding clusters. We investigated the differences in the electric-field response of the density of states (DOS) peak of the proton 1s orbital and the number of electrons on the proton for the cases of a diamond cluster and a graphite cluster. These differences are attributable to the differences in the overlap between the proton 1s orbital and the surface orbitals. We discuss the relationship between this electric-field effect on the DOS peak, critical points of the Q-$<n>$ curve and two characteristic properties of diamond electrodes, that is, low background currents and wide potential windows.

Boron-doped diamond is one of the most attractive and applicable electrode materials because of its chemical stability, high thermal conductivity, low background current (low capacitance), high rate of electron transfer in electrochemical reactions and very high overpotentials for both hydrogen and oxygen evolution in aqueous electrolytes (wide potential window). Many investigations of these characteristic properties of boron-doped diamond electrodes have been published,[1–16] and remarkable progress has recently been made in the application of boron-doped diamond electrodes.[17–19]

According to recent experimental studies,[5–7] the width of the potential window of boron-doped diamond electrodes is 3.5 V in 0.1 M H_2SO_4, as opposed to 2.8 V for glassy carbon and 2.2 V for the HOPG (Highly Oriented Pyrolytic Graphite) basal plane in 0.1 M H_2SO_4. These differences are attributable to the electronic structure of each electrode surface. That is, the surface of carbon-based electrodes other than diamond electrodes is basically a π-orbital system, whereas the diamond electrode surface consists of sp^3 carbons, which results in weak interactions between the diamond surface and adsorbates. Generally, both hydrogen and oxygen evolution in aqueous electrolytes consist of multi-step reactions involving adsorption processes on the electrode surfaces. One therefore would expect that higher overpotentials are necessary for hydrogen and oxygen evolution in the vicinity of electrode surfaces that interact weakly with adsorbates, such as diamond electrodes. However, the origin of the wide potential window of boron-doped diamond electrodes still remains to be discovered. Their electronic properties, such as the wide potential window, high rate of electron transfer and low capacitance, have also been explained only intuitively. It is necessary to investigate these problems in more detail and to make further analytical progress in the application of boron-doped electrodes, as well as to understand their properties.

With regard to recent theoretical approaches to diamond electrodes, Anderson and Kang[20] investigated hydrogen evolution on a diamond cathode surface by using ab initio calculations, with the assumption that the mechanism $H^+(aq) + C–H(\text{diamond surface}) + e^- \rightarrow H_2 + C_{radical}(\text{diamond surface})$ is the hydrogen evolution mechanism. They modeled a diamond cathode surface and $H^+(aq)$ by alkane molecules (methane and isobutane) and H_3O^+, respectively. A cathode was represented by placing a donor molecule in the system 10 Å away from the alkane molecule. According to their calculations, electron transfer in hydrogen evolution on the diamond cathode surface is expected to occur simultaneously with a transition state. The calculations show that the activation energy decreases as the potential becomes more negative. With regard to carbon radicals formed in the surface after hydrogen evolution, the authors suggested that C–H bonds on the diamond surface should be formed again by discharging $H^+(aq)$ on the carbon radicals. In their study, the interaction between the C–H bond (diamond surface) and the O–H bond (oxonium ion) is assumed as the initial state of hydrogen evolution on the diamond cathode sur-

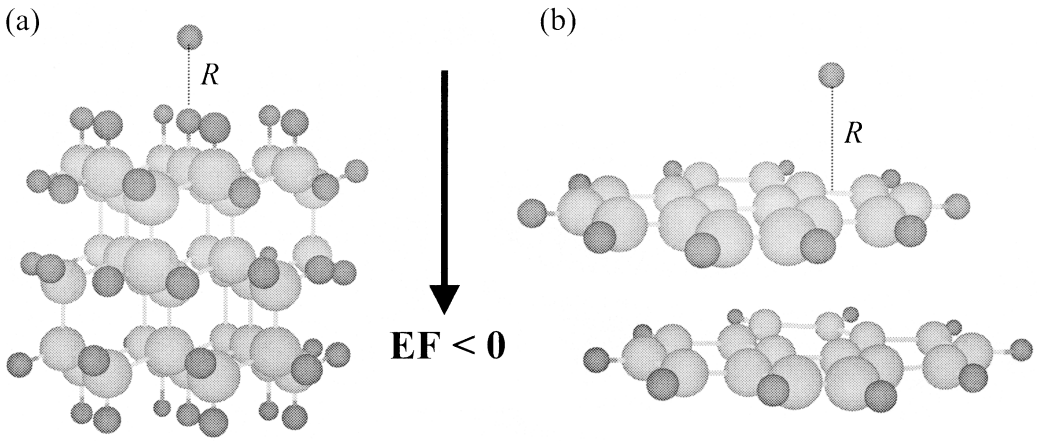

Fig. 1. Models of the carbon-based electrode surface: (a) a model cluster for the non-doped diamond electrode surface; and (b) a model cluster for the graphite electrode surface. *R* represents the distance between the proton and the surface.

face. However, such an interaction is very weak and it is still unclear whether this interaction is able to play a role as the initial stage of the hydrogen evolution in solution, where thermal motion is vigorous.

In this study, in order to understand the microscopic origin of the wide potential window and low background current of diamond electrodes, we study the electron transfer between a proton and carbon-based electrodes (diamond and graphite electrodes), instead of investigating directly the process of hydrogen and oxygen evolution. The effect of the thermal motion of solvent molecules was taken into account by adopting a thermo-bath model. With regard to the basic electronic structure of our model systems, we performed first-principle calculations by using density functional theory (DFT). As a representation of the electrodes, we applied a uniform electric field to our model systems, and we investigated the electric-field effect on the electron transfer between a proton and carbon-based electrodes. Finally we strove to understand the nature of the electronic properties of boron-doped diamond electrodes, especially their low background current and wide potential window.

Method

1. Calculation Models. In this study, we did not take the structure of the solution directly into account, but we approximated the overall electrostatic effects that result from both the structure of the solution in the vicinity of electrodes and the configuration of the electrode surface by a uniform electric field. However, the structure and orientation of adsorbates at interfaces may reflect the microscopic structure of the electric field (EF). Therefore, it is necessary to note that our model calculation is the "first step" in the investigation of the EF effects on the electron-transfer process at electrodes.

Diamond and graphite electrode surfaces have been modeled based on $C_{38}H_{44}$ and $C_{32}H_{20}$ clusters, respectively (Fig. 1). For diamond surfaces, two types of surface-forms, hydrogenated and oxygenated, are well-known. In this study, we adopted the hydrogenated surface-form as a model of diamond electrode surfaces to simplify our theoretical analysis. The nearest C–C distances in the diamond and graphite electrode model clusters are fixed at 1.54 Å and 1.42 Å, respectively. The C–H distances in the diamond and graphite clusters are fixed at 1.07 Å and 1.09 Å, respectively. In the actual boron-doped diamond electrodes, the concentration of boron atoms is about 10^{21} cm^{-3}, which corresponds to the density of one boron atom per 100–1000 carbon atoms. However, to investigate the effects of doping boron atoms on the electronic structure of the diamond cluster, we have used a diamond cluster containing four boron atoms inside the cluster. In this boron-doped diamond cluster, we assume that the doped boron atoms are not segregated on the diamond electrode surface. Although this population of boron atoms in our model is rather high in comparison with that in a realistic case, it is necessary to use a high population to clarify the effect of boron doping. For the graphite cluster, the distance between the first and second layer is fixed at 3.01 Å. We have adopted a proton as an adsorbate and assumed reduction of the proton in the vicinity of the electrodes in our models. According to our preliminary calculations, the interaction between the proton and the diamond (graphite) cluster was obtained to be largest at the C–H top (6-fold hollow) site. We therefore concentrate our study on these interaction sites.

In our DFT calculations, we have used the B3LYP/6-31G method, which uses a Becke-style 3-parameter DFT,[21] the Lee–Yang–Parr correlation functional.[22] Polarization functions were added to the basis set of hydrogen atoms. We used a Hamiltonian, as shown in Eq. 1, to obtain Kohn–Sham self-consistent field solutions of the electronic wave functions. The Hamiltonian, in the presence of the electric field, $\vec{F}$, is given by

$$H(\vec{F}) = H(\vec{0}) + e\vec{F}\cdot\sum_i \vec{r_i} - e\vec{F}\cdot\sum_j Q_j \vec{R_j} \qquad (1)$$

where $H(\vec{0})$ is the field-free Hamiltonian, Q_j is the charge on the atomic nuclei, and r_i and R_j are electron and nuclear coordinates, respectively. The second term denotes interactions between the electric field and electrons, and the third term represents interactions between the field and atomic nuclei. This scheme may be called the "finite-field DFT method". This electric-field Hamiltonian has been widely used for HF-SCF calculations.[23–33] The finite electric field is in a direction that is

normal to the surface, and the magnitude that we have adopted is 0.01 au, which correspond to 5.14×10^7 V/m. The sign of the electric field is chosen so that a positive sign induces a negative charge on the adsorbates (Fig. 1). In the case of EF < 0, the model clusters correspond to a cathode electrode, and in this study we imposed an electric field having this direction to study the reduction of a proton in the vicinity of the electrode.

To investigate donor–acceptor interactions between the orbitals of the proton and the electrode and to obtain their overlap integrals, we carried out an NBO (Natural Bond Orbital) analysis.[34,35] The purpose of obtaining overlap integrals is to estimate the coupling constants, which are necessary in carrying out the Anderson–Newns Hamiltonian analysis as mentioned in the next section. We will explain and discuss the coupling constants in the next section in detail. All first-principle calculations and NBO analyses were carried out using the Gaussian94 and Gaussian98 program packages.[36]

2. Anderson–Newns Hamiltonian Analysis. For the purpose of studying the electron transfer process between a proton and the carbon electrodes, we have analyzed our model systems with an Anderson–Newns Hamiltonian using the DFT electronic properties of the system. The application of Anderson–Newns Hamiltonian analysis to electrode surfaces has been advanced by Schmickler et al.[37–43] Then Sebastian[44] suggested an Anderson–Newns Hamiltonian analysis containing the effects of electron-hole excitations in metal electrodes. Voth et al.[45–53] and Nozik et al.[54,55] developed a hybrid method of Anderson–Newns Hamiltonian analysis and computer simulations to investigate electron transfers at various surface–liquid interface systems.

The Anderson–Newns Hamiltonian[44] is

$$H = H_e(Q) + H_{solv} \tag{2}$$

where $H_e(Q)$ and H_{solv} are the electronic part of the system, an adsorbate and an electrode surface, and the solvent part, respectively. In this model, the solvent is represented as a collection of harmonic oscillators,

$$H_{solv} = \sum_v \frac{1}{2}\left(p_v^2 + \omega_v^2 q_v^2\right) \tag{3}$$

where p_v, q_v and ω_v are the vth oscillator's momentum, position and frequency, respectively. The electronic part $H_e(Q)$ is a function of Q and the system interacts with the solvent system through this general solvent coordinate Q,

$$Q = \sum_v C_v q_v \tag{4}$$

where C_v are constants. $H_e(Q)$ is given by

$$H_e(Q) = \varepsilon_a n_a + Q n_a + \sum_k \left(\varepsilon_k n_k + V_{ak} c^+{}_a c_k + V_{ka} c^+{}_k c_a\right) \tag{5}$$

where ε_a stands for the energy of orbital $|a\rangle$ on the adsorbate, ε_k stands for the energy of orbital $|k\rangle$ on the electrode, c and c^+ are annihilation and creation operators, n is the occupation number operator, and V is the coupling constant representing the interaction between $|a\rangle$ and $|k\rangle$, respectively. In the Hamiltonian (5), the interaction between the adsorbate and the thermal motion of the solvent is represented by the term Qn_a and the electronic exchange interactions between the adsorbate and electrode are expressed by the terms $V_{ak}c^+{}_a c_k$ and $V_{ka}c^+{}_k c_a$. In this study, we have adopted a proton as an adsorbate and treated just one electron, so we have not taken account of the spin of the electrons.

In order to obtain several important physical quantities, it is useful to derive the density of states (DOS) of the electronic state on the adsorbate. By using Green's function, one can obtain the DOS of the electronic state on the adsorbate ρ_a as a function of the electron energy level ω and the general solvent coordinate Q,[44] that is

$$\rho_a(\omega,Q) = \frac{\Delta(\omega)}{\pi\left\{(\omega - \varepsilon_a - Q - \Pi(\omega))^2 + \Delta(\omega)^2\right\}} \tag{6}$$

where

$$\Delta(\omega) = \pi \sum_k |V_{ak}|^2 \delta(\omega - \varepsilon_k) \tag{7}$$

$$\Pi(\omega) = \frac{1}{\pi}\left[\textit{principal value} \int_{-\infty}^{\infty} \frac{\Delta(\omega')}{\omega - \omega'} d\omega'\right]. \tag{8}$$

Generally, Δ and Π are treated as parameters. However, in our approach, we have used a Lorenz function with a relatively narrow width as a substitute for the δ function in (7) and have succeeded in treating Δ and Π as functions of ω. The coupling constants V_{ak} have been estimated by using a Wolfsberg–Helmholz approximation, which is given by

$$V_{ak} = \frac{1}{2} K S_{ak} (\varepsilon_k + \varepsilon_a) \tag{9}$$

where S_{ak} stands for the overlap integral between $|a\rangle$ and $|k\rangle$, and K is a positive constant (> 1.0 in the case of dealing with most hydrocarbon molecules), which is assumed to be 1.0 in our study. The overlap integrals have been calculated by carrying out the NBO analysis. In this analysis, canonical molecular orbitals and Kohn–Sham orbitals obtained by electronic state calculations are localized based on the NBO theory to be changed to NBO, and one can investigate donor–acceptor interactions between NBOs in the system.

As one of the most important physical quantities obtained from the DOS, $\rho_a(Q)$, we have calculated the expectation value for the number of electrons on the adsorbate $\langle n_a(Q)\rangle$. This can be calculated numerically:

$$\langle n_a(Q)\rangle = \int_{-\infty}^{\varepsilon_F} \rho_a(\omega,Q) d\omega \tag{10}$$

where ε_F is the Fermi energy of the electrode. We have adopted the HOMO of the clusters as the Fermi energy in (10).

In our study, based on the method discussed above, we have analyzed the DOS and the number of electrons on the adsorbate and the changes effected by the solvent thermal motion and by an imposed electric field to investigate the difference between the properties of boron-doped diamond electrodes and graphite electrodes.

Results and Discussions

1. DFT Calculations. In this section, we pay attention to

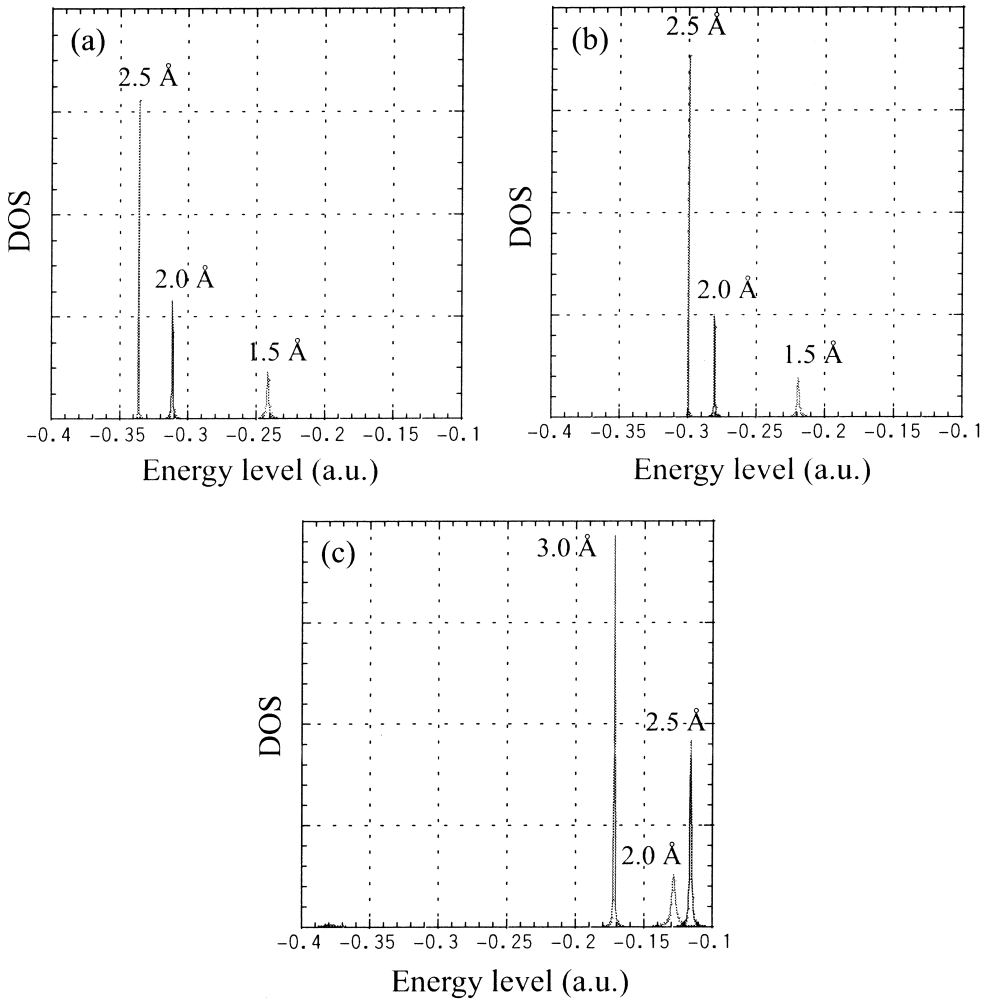

Fig. 2. DOS for the proton 1s orbital $\rho_a(\omega, Q = 0)$ interacting with model clusters: (a) the non-doped diamond cluster (R = 1.5, 2.0 and 2.5 Å); (b) the boron-doped diamond cluster (R = 1.5, 2.0 and 2.5 Å); and (c) the graphite cluster (R = 2.0, 2.5 and 3.0 Å).

the HOMO-LUMO gaps. Qualitatively speaking, the HOMO-LUMO gap of cluster-modeled electrodes can be used to estimate band-gaps of the corresponding real electrode. The HOMO-LUMO gap of our graphite cluster is calculated to be 79.4 kcal/mol, only 0.7 kcal/mol larger than the well-known experimental value of the band-gap of graphite. In the cases of non-doped diamond and boron-doped diamond clusters, the gap is 184.3 kcal/mol and 16.5 kcal/mol, respectively, where this reduction of the HOMO-LUMO gap is caused by the lowering of the energy level of the LUMO induced by the empty p orbitals of doped boron atoms. This may explain the high conductivity of boron-doped diamond electrodes. However, the experimentally known band-gap of non-doped diamond is approximately 125.5 kcal/mol and the energy gap of boron-doped diamond between the acceptor level and the valence band is approximately 8.1 kcal/mol. It may be objected that our clusters are too small to reproduce the band-gap of real electrodes. However, the band-gap is related to the conductivity of the electrode, and it may be thought that the electrochemical phenomena in the vicinity of electrode surfaces are mainly affected by the electronic structures of the electrode surfaces. Therefore, in the next section, we will discuss the results obtained from Anderson–Newns Hamiltonian analysis based on these cluster models.

With regard to the interaction distance between the proton and the surfaces, a strong interaction between the surface and the proton appeared at the surface–proton distance d = 2.0 Å and 1.5 Å, respectively, for the diamond cluster and for the graphite cluster. This difference will be taken into account in the discussion on the changes of the DOS of the proton orbital in Sec. 2-1.

2. Anderson–Newns Hamiltonian Analysis. 2-1. DOS of Proton Orbital Adsorbed on Carbon-Based Electrodes: Figure 2 shows the DOS of the proton orbital $\rho_a(\omega, Q = 0)$ as a function of the proton-surface distance. According to NBO analysis, in the case of the diamond cluster (Figs. 2a and b), the DOS peak results from the interaction between the σ_{C-H} orbitals of the surface and the proton orbital, while in the case of the graphite electrode (Fig. 2b), the DOS peak is attributable to the interaction with the π_{C-C} orbitals of the surface. No other DOS peaks are found, and this shows that the proton interacts mainly with the orbitals of the first layer of the cluster.

First, we will discuss the effect of boron atoms doped in the diamond cluster on the DOS of the proton orbital. According to Figs. 2a and b, the boron doping shifts the positions of the DOS peaks and there are only small effects on the shapes of

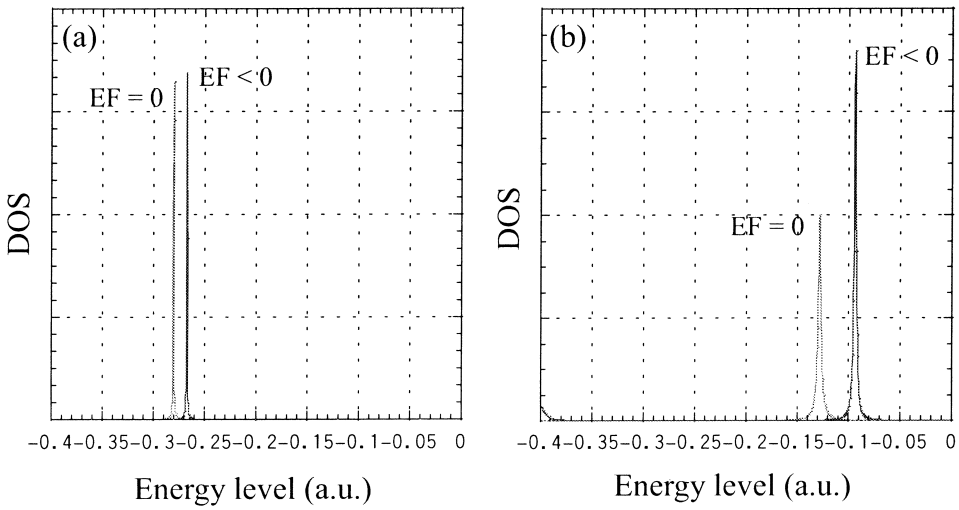

Fig. 3. DOS for the proton 1s orbital $\rho_a(\omega, Q = 0)$ interacting with model clusters under EF = 0 and EF < 0: (a) the non-doped diamond cluster (R = 2.0 Å); and (b) the graphite cluster (R = 2.0 Å).

the DOS. These results indicate that boron doping in the diamond electrode does not have a direct effect on the interaction between the surface and adsorbates, and that the important factor affecting the interaction may be the electronic structure of the electrode surface. In the following, we will compare the non-doped diamond cluster and the graphite cluster.

According to Fig. 2, the shorter the proton–surface distance R, the greater the width of the DOS spectra becomes. For the diamond electrode model, the position of the DOS peak shifts toward a high energy level as the adsorbate–surface distance becomes shorter. With regard to the graphite electrode model, however, the change of the position of the DOS peak is irregular, in contrast to the case of the diamond electrode model. According to our DFT calculations, when the proton and the graphite cluster interact around R = 1.5–2.5 Å, almost one electron transfers from the graphite cluster to the proton, and the proton takes not a cationic but a hydrogen-like form because of the strong interaction between the proton and the graphite surface. This drastic change in the electronic structure of the proton–graphite cluster interaction system around R = 1.5–2.5 Å is considered to produce the lack of correlation between R and the position of the DOS peak.

In Fig. 3, the changes of the DOS of the proton orbital $\rho_a(\omega, Q = 0)$ by the direction of the electric field for each cluster are shown. The adsorption distance is fixed at 2.0 Å for both the diamond and the graphite clusters. In the case of the diamond cluster, this distance, 2.0 Å, corresponds to the strongest interaction distance between the surface and the proton. On the other hand, the strongest interaction distance between the graphite surface and the proton was obtained at 1.5 Å, as mentioned in Sec. 1. In this case, however, the proton 1s orbital is united with the graphite surface orbitals because of the strong interaction between those orbitals, and we were not able to obtain the overlap integral between the graphite surface and the proton. Therefore, in this section, we adopted 2.0 Å as the proton–graphite interaction distance. The position of the DOS peak for the graphite surface shifts significantly on imposing a negative electric field (see Fig. 3b). On the other hand, the change of the DOS peak for the diamond cluster is less sensitive to the imposed electric field. The width of the DOS peak shift is approximately 0.01 au and 0.04 au for the diamond and the graphite cluster, respectively. According to Eq. 6, the position of the DOS peak mainly depends on the energy level of the proton orbital ε_a. In order to understand the cause of this difference in the shift width of the DOS peak induced by an electric field, let us attempt to consider it from the viewpoint of orbital interaction theory.

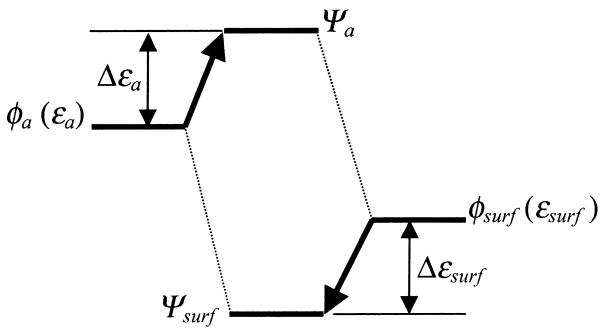

Fig. 4. Diagram for the energy-level shifts of two orbitals ϕ_a and ϕ_{surf} interacting with each other. ε_a and ε_{surf} represent the energy level of orbitals ϕ_a and ϕ_{surf}, respectively ($\varepsilon_a > \varepsilon_{surf}$), Ψ_a and Ψ_{surf} represent orbitals that are newly formed through the interaction between orbitals ϕ_a and ϕ_{surf}, and $\Delta\varepsilon_a$ and $\Delta\varepsilon_{surf}$ represent the shift width of ε_a and ε_{surf} induced through the interaction between orbitals ϕ_a and ϕ_{surf}.

When two orbitals, ϕ_a and ϕ_{surf}, having different energy levels ($\varepsilon_a > \varepsilon_{surf}$), interact with each other, the energy level of each orbital shifts as shown in Fig. 4. These shift-widths, $\Delta\varepsilon_a$ and $\Delta\varepsilon_{surf}$, are calculated as

$$\Delta\varepsilon_a = \frac{(V - \varepsilon_{surf}S)^2}{\varepsilon_a - \varepsilon_{surf}} \tag{11a}$$

$$\Delta\varepsilon_{surf} = \frac{(V - \varepsilon_a S)^2}{\varepsilon_a - \varepsilon_{surf}} \tag{11b}$$

where S (> 0) and V are the overlap integral and the coupling

constant between the orbital ϕ_a and ϕ_{surf}, respectively. Here we assume that S, V, ε_a and ε_{surf} change into $S + \Delta S$, $V + \Delta V$, $\varepsilon_a + \Delta\varepsilon_a^{EF}$ and $\varepsilon_{surf} + \Delta\varepsilon_{surf}^{EF}$ by imposing an electric field. Based on the basic orbital interaction theory, the coupling constant can be related to K as $V = K\varepsilon_a S$ ($= K\varepsilon_{surf}S$), where K is the same as the one in Eq. 9. Note that S is a measure of the strength of the surface–adsorbate interaction, and ΔS, $\Delta\varepsilon_a$ and $\Delta\varepsilon_{surf}$ show the sensitivity of the interaction to the electric field. The shift-widths of the energy levels of orbitals Ψ_a and Ψ_{surf}, which are newly formed through the interaction between ϕ_a and ϕ_{surf} induced by the electric field, $\Delta\Delta\varepsilon_a$ and $\Delta\Delta\varepsilon_{surf}$, are obtained as

$$\begin{aligned}\Delta\Delta\varepsilon_a &= \Delta\varepsilon_{a(EF<0)} - \Delta\varepsilon_{a(EF=0)} \\ &\cong \varepsilon_a^2(K-1)S^2\left\{\frac{2\left(\Delta\varepsilon_a^{EF}/\varepsilon_a + \Delta S/S\right)}{\varepsilon_a - \varepsilon_{surf}} - \frac{\Delta\varepsilon_a^{EF} - \Delta\varepsilon_{surf}^{EF}}{\left(\varepsilon_a - \varepsilon_{surf}\right)^2}\right\} \qquad (12a)\end{aligned}$$

$$\begin{aligned}\Delta\Delta\varepsilon_{surf} &= \Delta\varepsilon_{surf(EF<0)} - \varepsilon_{surf(EF=0)} \\ &\cong \varepsilon_{surf}^2(K-1)S^2\left\{\frac{2\left(\Delta\varepsilon_{surf}^{EF}/\varepsilon_{surf} + \Delta S/S\right)}{\varepsilon_a - \varepsilon_{surf}} - \frac{\Delta\varepsilon_a^{EF} - \Delta\varepsilon_{surf}^{EF}}{\left(\varepsilon_a - \varepsilon_{surf}\right)^2}\right\} \qquad (12b)\end{aligned}$$

where the second-order terms are neglected. Eq. 12a (12b) indicates that $\Delta\Delta\varepsilon_a$ ($\Delta\Delta\varepsilon_{surf}$) depends on S, ΔS and $\Delta\varepsilon_a$ ($\Delta\varepsilon_{surf}$).

Table 1 shows the differences in S, ΔS, $\Delta\varepsilon_a$ and $\Delta\varepsilon_{surf}$ for the cases of the diamond and graphite clusters. The difference in S, which is greater than those in ΔS and $\Delta\varepsilon$ (the graphite cluster $>$ the diamond cluster), may be considered as a dominant factor in Eqs. 12a and b. ΔS for the graphite cluster is also larger than that for the diamond cluster, indicating that the response of the graphite surface orbitals, $\pi_{C\text{–}C}$, to the electric field is greater than that for the diamond surface orbitals, $\sigma_{C\text{–}H}$. However, the difference in ΔS is not a dominant factor in Eqs. 12a and b ($\Delta S/S \cong 0$). According to our calculation, the energy level of the proton 1s orbital is not shifted by the imposed electric field ($\Delta\varepsilon_a = 0$). Then Eq. 12a finally has the following form:

$$\Delta\Delta\varepsilon \cong 2\varepsilon_{surf}(K-1)S^2\frac{\Delta\varepsilon_{surf}^{EF}}{\varepsilon_a - \varepsilon_{surf}}. \qquad (13)$$

Therefore, the reason that the difference in the shift width of the DOS for the graphite cluster is larger than in the case of the diamond cluster is that the surface–adsorbate overlap integral, i.e., the surface–adsorbate interaction, for the graphite cluster is greater than in the case of the diamond cluster.

2-2. Electron Transfers between Proton and Carbon-Based Electrodes: In this section, the number of electrons in the proton 1s orbital interacting with the diamond and graphite surfaces is discussed with respect to a function of the general solvent coordinate Q (Q-<n> curves). The Q-<n> curves obtained from Eq. 10 for three different proton–surface distances are shown in Fig. 5, and electric field effects are shown in Fig. 6. In general, the number of electrons on the adsorbate, <n>, changes like a step function with respect to the thermal motion of the solvent, Q. Considering electron transfers in actual systems based on Q-<n> curves, electron transfers occur when the critical points of the Q-<n> curves are located in the energy range of the thermal motions of solvent molecules around the adsorbate and the surface. The critical points of the Q-<n> curves depend on both the peak positions of the DOS spectrum and the HOMO energy level of the cluster interacting with the adsorbate (see Eqs. 6 and 10). In the case that a proton does not interact with a surface, the Q-<n> curve takes exactly a step-function form. The energy difference between the critical point and the point $Q = 0$ (ΔQ) corresponds to the energy that is required for an electron transfer from the surface to the proton, where the energy is supplied by the thermal motion of the solvent molecules around the proton and interfacial to the surface.

Table 1. Comparison between the Cases of the Diamond and Graphite Clusters, in Overlap Integral between the Proton and the Surface Orbital, Difference in the Overlap Integral between the Cases of EF = 0 and EF < 0 and Difference in ε_{surf} between the Cases of EF = 0 and EF < 0

	S[a)]	ΔS[b)]	$\Delta\varepsilon_{surf}^{EF}$ (a.u.)[c)]
Diamond cluster	0.1685	0.0005	0.0049
Graphite cluster	0.2598	0.0081	−0.0121

a) Overlap integral between the proton and the surface orbital.
b) Difference in S between the case of EF = 0 and EF < 0.
c) Difference in ε_{surf} between the case of EF = 0 and EF < 0.

First, we discuss the dependence of the Q-<n> curves on the proton–surface distance. Schmickler and co-workers[44,45] treated the term of solvent motion effects as a function of the adsorbate–surface distance, based on the fact that the interaction energy of an adsorbate with solvent molecules changes with the adsorbate–surface distance.[57] Therefore, with regarding to the thermal motion of solvent molecules in our model, it is necessary to multiply Q by some scaling factor. In this study, however, we discuss the Q-<n> curves without scaling Q.

According to Fig. 5a, when $Q = 0$, the number of electrons on the adsorbed proton is not zero because of a charge transfer from the clusters to the proton. In the case of the diamond cluster, the number of electrons on the adsorbate decreases on increasing the proton–surface distance. The same tendency is found for the graphite cluster (see Fig. 5b). Paying attention to the shapes of the curves, one sees from Fig. 5a that the Q-<n> curve takes a smoother form as the proton–surface distance decreases. This tendency results from the width of the DOS peak of the proton 1s orbital at each proton–surface distance, that is, the magnitude of the proton–surface interaction. According to Fig. 5b, on the other hand, there is no such correlation between the critical point of the Q-<n> curve and the proton–graphite surface distance. In our DFT calculations for the proton–graphite interaction system, the number of electrons on the proton changes drastically at $R = 2.5$ Å. That is, when the proton–graphite distance is less than 2.5 Å, almost one electron transfers from the graphite cluster to the proton, and a

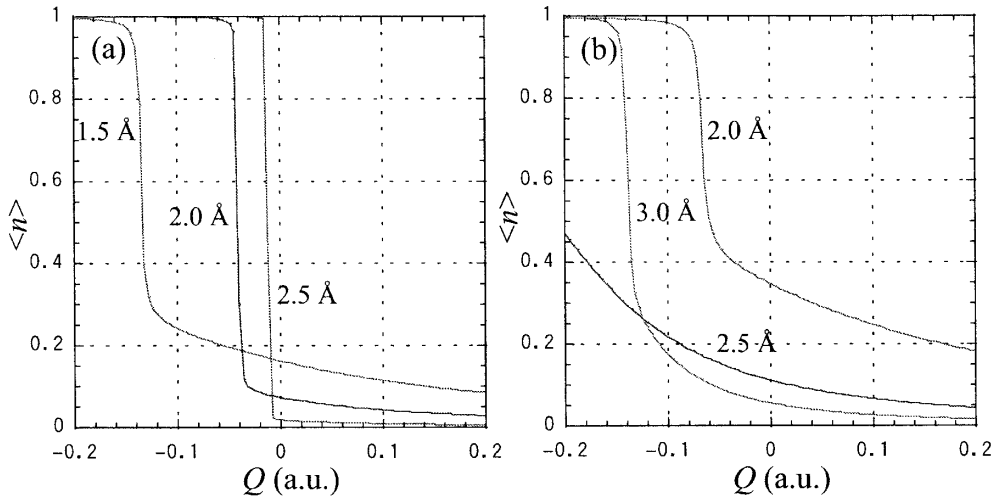

Fig. 5. Q-<n> curves for the proton 1s orbital $\rho_a(Q)$ interacting with model clusters: (a) the non-doped diamond cluster (R = 1.5, 2.0 and 2.5 Å); and (b) the graphite cluster (R = 2.0, 2.5 and 3.0 Å).

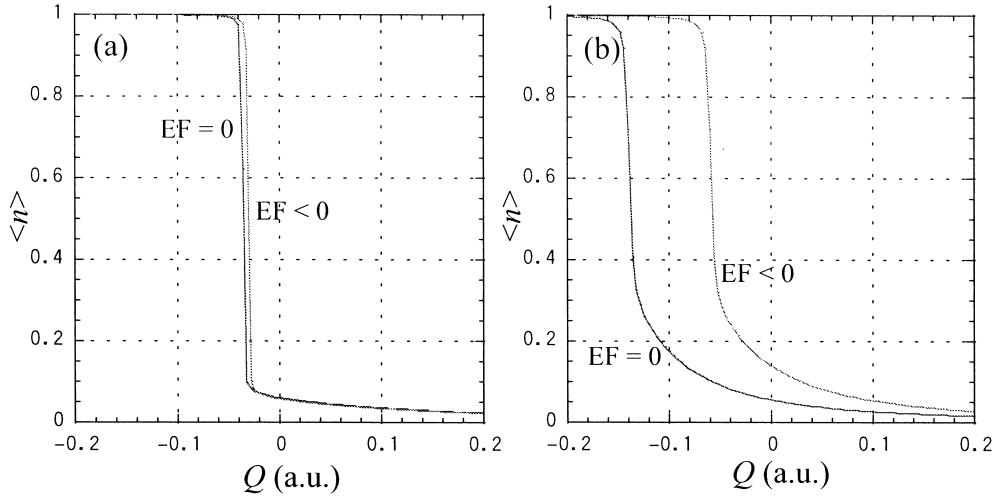

Fig. 6. Q-<n> curves for the proton 1s orbital $\rho_a(Q)$ interacting with model clusters under EF = 0 and EF < 0: (a) the non-doped diamond cluster (R = 2.0 Å); and (b) the graphite cluster (R = 3.0 Å).

non-adiabatic change also occurs in the proton–graphite interaction, which is considered to be the cause of the lack of correlation between the critical point of the Q-<n> curve and the proton–graphite surface distance.

Next, we discuss the dependence of the Q-<n> curve on the imposed electric field. The proton–surface distance for the diamond cluster is fixed at 2.0 Å. This proton–diamond distance is at the minimum point of the interaction energy. With regard to the proton–graphite distance, we chose not the minimum point of the proton–graphite interaction energy (2.0 Å) but 3.0 Å, because at R = 2.0 and 2.5 Å hybridization of the proton 1s orbital and the π orbitals of the graphite cluster occurs, preventing us from calculating the overlap integrals.

According to Fig. 6b, the critical point of the Q-<n> curve for the graphite surface shifts significantly on applying a negative electric field, while that of the diamond surface is less sensitive to the electric field, as shown in Fig. 6a. The shift-widths for the diamond cluster and the graphite cluster are approximately 0.01 au and 0.09 a.u., respectively. These tendencies directly reflect the DOS of the proton orbital shown in Fig. 3a and b. That is, the electron transfer between the electrode surface and the adsorbate is influenced greatly by the response of the orbitals in the surface to the imposed electric field, which may be related to the fact that diamond electrodes generally have a wide potential window. As mentioned above, the electron transfer from the surface to the proton occurs when the critical point of the Q-<n> curve is moved by an imposed bias, an electric field in our model, to reach the energy range of the motion of the solvent molecules around the proton and the surface (see Fig. 7). Therefore, if the shift width of the critical point of the Q-<n> curve induced by an imposed electric field is narrow, as in the case of the diamond cluster, a stronger electric field is necessary in order that the critical point may reach the energy range of Q, where electron transfer occurs from the surface to the proton. Our results for the shift-widths of the critical point of the Q-<n> curves for the two model clusters do

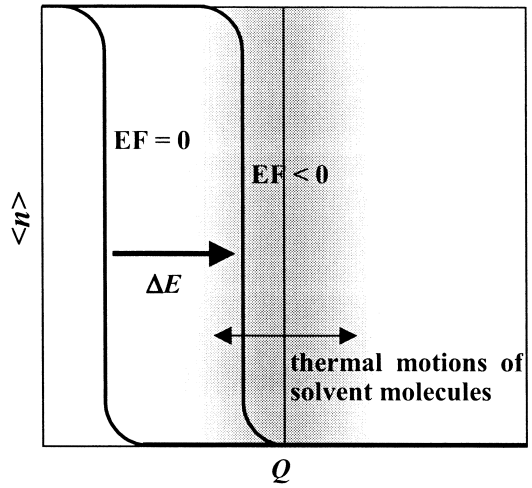

Fig. 7. Diagram of the relationship between the shift of the Q-<n> curve induced by an imposed electric field and the energy range of thermal motions of solvent molecules in the vicinity of the surface. Electron transfer from the surface to the adsorbate occurs when the critical point of the Q-<n> curve is moved by an imposed electric field and reaches the energy range of the motion of solvent molecules around the adsorbate and the surface.

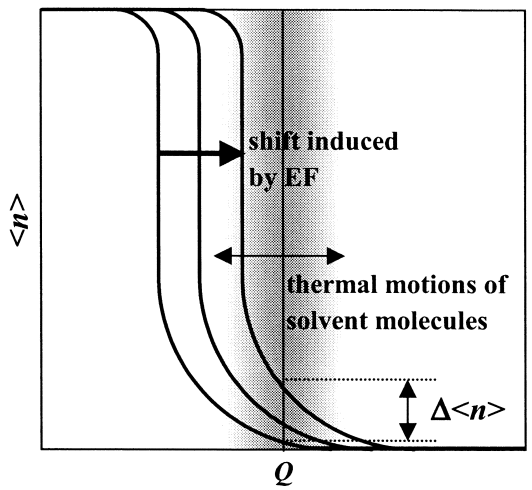

Fig. 8. Diagram for relationship between the shift of the Q-<n> curve induced by an imposed electric field and the energy range of thermal motions of the solvent molecules in the vicinity of the surface. Δ<n> represents the change in width of <n> around $Q = 0$. In the case that <n> around $Q = 0$ is small until the critical point of the Q-<n> curve reaches the solvent motion range, it corresponds to a low background current.

not conflict with the actual difference between the diamond electrodes and the graphite electrodes. As mentioned above, the change in the Q-<n> curve is related to the response of the orbitals in the surface; therefore, the fact that the diamond electrodes have a wider potential window than the graphite electrodes may be related to the difference in the response of the surface orbitals to an imposed electric field for the two carbon-based electrodes.

Here, let us pay attention to <n> around $Q = 0$. In the case that the critical point of the Q-<n> curve does not yet reach the energy range of thermal motions of the solvent molecules in spite of imposing an electric field, it is considered that <n> around $Q = 0$ will be relevant to the background current (see Fig. 8). As is well-known, with regard to the cause of the background current, several factors are important, for example, the reorientation of the solvent molecules in the vicinity of the electrode surface and the specific adsorption of ions in solution at the electrode surface and so on. Here, we will try to explain the background current from the viewpoint of the possibility of electron transfer from the electrode surface to the reductant (here, the expectation value for the number of electrons, <n>). In the case of the graphite cluster (Fig. 6b), the increase in the number of electrons on the proton induced by the electric field, Δ<n>, is significantly greater around $Q = 0$. On the other hand, in the case of the diamond cluster (Fig. 6a), Δ<n> induced by the electric field is not found and <n> around $Q = 0$ remains low. This difference between the cases of the diamond and graphite clusters is due to the difference in the width of the corresponding DOS peaks, which become wider as the interaction between the adsorbate and surface becomes stronger. <n> around $Q = 0$ for the diamond model remains low even when an electric field is imposed, corresponding to a low background current (see Fig. 8). Our result therefore shows that a weak interaction between the adsorbate and the diamond surface causes a low background current for the diamond electrode.

Conclusions

In this study, we have tried to explain the nature of the characteristic properties of boron-doped diamond electrodes, particularly the wide potential window. We discussed the electron transfer process between the diamond surface and H^+ based on Anderson–Newns Hamiltonian analysis. To obtain the necessary data for carrying out the analysis, we calculated the electronic structures of our models by the "finite-field DFT method" at the level of B3LYP/6-31G. We adopted the (boron-doped and non-doped) diamond and graphite clusters as the corresponding surface model, and a proton was adopted as the adsorbate.

By investigating the shift of the DOS peak of the proton 1s orbital induced by the imposed electric field, we explained two characteristic properties of the diamond surface: a low background current and a wide potential window. We found that, in the case of the diamond cluster, the change in the number of electrons in the range around $Q = 0$ induced by the imposed electric field is almost zero and maintains a low value. This is caused by the narrow width of the corresponding DOS peak, which reflects the weak interaction between the proton and the diamond surface. We have shown that the weak proton–diamond interaction results in the low background current of the diamond electrode.

We also found that the position of the DOS peak for the graphite surface shifts more significantly by imposing a positive electric field than for the diamond cluster. Based on orbital interaction theory, we showed that this difference in the response of the DOS peak to an imposed electric field results from the difference in the magnitude of the overlap integral be-

tween the proton orbital and the surface orbital (the graphite cluster > the diamond cluster). It was also found that the critical points of the Q-$\langle n \rangle$ curves also change according to the position of the corresponding DOS peaks, which indicates that the necessary energy for an electron to transfer from the diamond surface to the proton is larger than for the case of the graphite surface. This narrow shift width induced by the electric field for the diamond cluster may be related to the fact that a diamond electrode has a wide potential window; we showed the cause of the wide potential window of the diamond electrode.

This work is supported by a Grant-in-Aid for Scientific Research on Priority Area of "Electrochemistry of Ordered Interfaces" from the Ministry of Education, Science, Sports and Culture (#09237216, #10131213, #11740316), and by CREST (Core Research for Evolutional Science and Technology) of Japan Science and Technology Corporation (JST).

References

1 I. Iwaki, S. Sato, K. Takahashi, and H. Sakairi, *Nucl. Inst. Methods*, **209**/**210**, 1129 (1983).

2 G. M. Swain and R. Ramesham, *Anal. Chem.*, **65**, 345 (1993).

3 R. Tenne, A. Patel, K. Hashimoto, and A. Fujishima, *J. Electroanal. Chem.*, **347**, 409 (1993).

4 M. Awada, J. W. Strojek, and G. M. Swain, *J. Electrochem. Soc.*, **142**, L42 (1995).

5 S. Alehashem, F. Chambers, J. W. Strojek G. M. Swain, and R. Ramesham, *Anal. Chem.*, **67**, 2812 (1995).

6 P. Bouamrane, A. Tadjeddine, J. E. Butler, R Tenne, and C. Lévy-Clément, *J. Electroanal. Chem.*, **405**, 95 (1996).

7 H. B. Martin, A. Argoitia, U. Landau, A. B. Anderson, and J. C. Angus, *J. Electrochem. Soc.*, **143**, L133 (1996).

8 Q. Y. Chen, M. C. Granger, T. E. Lister, and G. M. Swain, *J. Electrochem. Soc.*, **144**, 3806 (1997).

9 N. Vinokur, B. Miller, Y. Avyigal, and R. Kalish, *J. Electrochem. Soc.*, **143**, L238 (1996).

10 J. Xu, M. C. Granger, Q. Chen, J. W. Strojek, T. E. Lister, and G. M. Swain, *Anal. Chem. News & Features*, **October 1**, 591A (1997).

11 L. Boonma, T. Yano, D. A. Tryk, K. Hashimoto, and A. Fujishima, *J. Electrochem. Soc.*, **144**, L142 (1997).

12 F. Bouamrane, A. Tadjeddine, R. Tenne, J. E. Butler, R. Kalish, and C. Lévy-Clément, *J. Phys. Chem. B*, **102**, 134 (1998).

13 L-F. Li, D. A. Totir, N. Vinokur, B. Miller, G. Chottiner, E. A. Evans, J. C. Angus, and D. A. Scherson, *J. Electrochem. Soc.*, **145**, L85 (1998).

14 T. Yano, D. A. Tryk, K. Hashimoto, and A. Fujishima, *J. Electrochem. Soc.*, **145**, 1870 (1998).

15 S. Nakabayashi, D. A. Tryk, A. Fujishima, and N. Ohta, *Chem. Phys. Lett.*, **300**, 409 (1999).

16 E. Popa, H. Notsu, T. Miwa, D. A. Tryk, and A. Fujishima, *Electrochem. and Solid-State Lett.*, **2**, 49 (1999).

17 T. N. Rao, I. Yagi, T. Miwa, D. A. Tryk, and A. Fujishima, *Anal. Chem.*, **71**, 2506 (1999).

18 C. E. Troupe, I. C. Drummomd, C. Graham, J. Grice, P. John, J. I. B. Wilson, M. G. Jubber, and N. A. Morrison, *Diamond Relat. Mater.*, **7**, 575 (1998).

19 S. Yoshihara, K. Shiozaki, T. Shirakawa, K. Hashimoto, D. A. Tryk, and A. Fujishima, *Electrochim. Acta*, **44**, 2711 (1999).

20 A. B. Anderson and D. B. Kang, *J. Phys. Chem. A*, **102**, 5993 (1998).

21 A. D. Becke, *J. Chem. Phys.*, **98**, 5648 (1993).

22 C. Lee, W. Yang, and R. G. Parr, *Phys. Rev. B*, **37**, 785 (1988).

23 B. Miehlich, A. Savin, H. Stoll, and H. Preuss, *Chem. Phys. Lett.*, **157**, 200 (1989).

24 X. Xu, D. Y. Wu, B. Ren, H. Xian, and Zhong-Qun Tian, *Chem. Phys. Lett.*, **311**, 193 (1999).

25 M. Head-Gordon and J. C. Tully, *Phys. Rev. B*, **46**, 1853 (1992).

26 A. B. Anderson, *J. Electroanal. Chem.*, **280**, 37 (1990).

27 D. K. Lambert, *J. Chem. Phys.*, **89**, 3847 (1988).

28 G. Pacchioni and P. S. Bagus, *Phys. Rev. B*, **40**, 6003 (1989).

29 P. S. Bagus, C. J. Nelin, K. Hermann, and M. R. Philpott, *Phys. Rev. B*, **36**, 8169 (1989).

30 P. S. Bagus, C. J. Nelin, W. Müller, M. R. Philpott, and H. Seki, *Phys. Rev. Lett.*, **58**, 559 (1989).

31 M. R. Philpott, P. S. Bagus, C. J. Nelin, and H. Seki, *J. Electron Spectrosc. Relat. Phenom.*, **45**, 169 (1987).

32 S. Holloway and J. K. Nørskov, *J. Electroanal. Chem.*, **161**, 193 (1984).

33 C. Korzeniewski, S. Pons, P. P. Schmidt, and M. W. Severson, *J. Chem. Phys.*, **85**, 4153 (1986).

34 J. P. Foster and F. Weinhold, *J. Am. Chem. Soc.*, **102**, 7211 (1980).

35 A. E. Reed, L. A. Curtiss, and F. Weinhold, *Chem. Rev.*, **88**, 899 (1988).

36 "*The Structure of Small Molecules and Ions*," ed by F. Weinhold and J. E. Carpenter, in, R. Naaman, and Z. Vager, Plenum, New York (1988), pp. 227.

37 M. J. Frisch, G. W. Trucks, H. B. Schlegel, P. M. W. Gill, B. G. Johnson, M. A. Robb, J. R. Cheeseman, T. Keith, G. A. Petersson, J. A. Montgomery, K. Raghavachari, M. A. Al-Laham, V. G. Zakrzewski, J. V. Ortiz, J. B. Foresman, J. Cioslowski, B. B. Stefanov, A. Nanayakkara, M. Challacombe, C. Y. Peng, P. Y. Ayala, W. Chen, M. W. Wong, J. L. Andres, E. S. Replogle, R. Gomperts, R. L. Martin, M. Gordon, C. Gonzalez, and J. A. Pople, "Gaussian94, Rev., D.1," Gaussian Inc., Pittsburgh, PA (1995).

38 W. Schmickler, *J. Electroanal. Chem.*, **100**, 533 (1979).

39 A. A. Kornyshev and W. Schmickler, *J. Electroanal. Chem.*, **185**, 253 (1985).

40 W. Schmickler, *Chem. Phys. Lett.*, **115**, 216 (1985).

41 A. A. Kornyshev and W. Schmickler, *J. Electroanal. Chem.*, **204**, 31 (1986).

42 W. Schmickler, *J. Electroanal. Chem.*, **100**, 533 (1979).

43 W. Schmickler, *J. Electroanal. Chem.*, **296**, 283 (1990).

44 W. Schmickler, *Chem. Phys. Lett.*, **237**, 152 (1995).

45 M. T. M. Koper and W. Schmickler, *J. Electroanal. Chem.*, **450**, 83 (1998).

46 W. Schmickler, *Chem. Phys. Lett.*, **317**, 458 (2000).

47 K. L. Sebastian, *J. Chem. Phys.*, **90**, 5056 (1989).

48 J. B. Staus and G. A. Voth, *J. Phys. Chem.*, **97**, 7388 (1993).

49 J. B. Staus, A. Calhoun, and G. A. Voth, *J. Chem. Phys.*, **102**, 529 (1995).

50 Y. G. Boroda and G. A. Voth, *J. Chem. Phys.*, **104**, 6168 (1996).

51 A. Calhoun and G. A. Voth, *J. Phys. Chem.*, **100**, 10746 (1996).

52 M. T. M. Koper and G. A. Voth, *Chem. Phys. Lett.*, **282**, 100 (1998).
53 Y. G. Boroda and G. A. Voth, *J. Electroanal. Chem.*, **450**, 95 (1998).
54 A. Calhoun, M. T. M. Koper, and G. A. Voth, *J. Phys. Chem. B*, **103**, 3442 (1999).
55 B. B. Smith and A. J. Nozik, *Chem. Phys.*, **205**, 47 (1996).
56 B. B. Smith and A. J. Nozik, *J. Phys. Chem. B*, **101**, 2459 (1997).
57 E. Spohr, *Chem. Phys. Lett.*, **207**, 214 (1993).